Room Temperature Synthesis of Two-Dimensional Multilayer Magnets based on α-Co^{II} Layered Hydroxides

Víctor Oestreicher,[a] Christian Dolle,[a] Diego Hunt,[b] Michael Fickert,[c] Gonzalo Abellán*[a,c]

[a] Instituto de Ciencia Molecular (ICMol). Universidad de Valencia. Catedrático José Beltrán 2, 46980, Paterna, Valencia (Spain)

[b] Departamento de Física de la Materia Condensada, GIyA. Instituto de Nanociencia y Nanotecnología, CNEA-CAC-CONICET.Av. Gral. Paz, 1650, San Martín, Buenos Aires (Argentina)

[c] Chair of Organic Chemistry II and Joint Institute of Advanced Materials and Processes (ZMP). Friedrich-Alexander-Universität Erlangen-Nürnberg (FAU). Nikolaus-Fiebiger Strasse 10, 91058 Erlangen and Dr.-Mack Strasse 81, 90762 Fürth (Germany)

Research on two-dimensional (2D) materials is one of the most active fields in materials science and nanotechnology. Among the members of the 2D family, layered hydroxides (LHs) represent an exceptional case of study due their unparalleled chemical versatility which allows the modulation of their physicochemical properties at will. Nowadays, LHs based on earth-abundant metals are key materials in the areas of energy conversion and storage, hybrid materials or magnetism. α-Co hydroxides (Simonkolleite-like structures) are promising phases with tuneable electronic and magnetic properties by ligand modification. However, even in the simple case of α-Co^{II} hydroxychlorides, the preparation of well-defined large 2D crystals is not straightforward, hindering the development of fundamental studies. Herein, we present the synthesis of 2D hexagonal crystals with outstanding size-thickness relationship (diameter > 5 μm and thickness of 20±7 nm) by a simple homogeneous synthesis taking place at room temperature. In structural terms, no differences are observed between our nanomaterials and those obtained hydrothermally. However, dynamic susceptibility measurements alert about different arrangements of the magnetic sublattices, which have been rationalized with structural DFT calculations. This work provides an extremely easy bottom-up method to obtain high-quality 2D crystals based on α-Co^{II} hydroxides, paving the way for the development of fundamental studies and applications.

Since the discovery of graphene, the field of two dimensional (2D) materials has become one of the most active research areas in materials science and nanotechnology.[1,2] As representative members of the 2D family, graphene, silicene, germanene and, more recently the pnictogens (black phosphorus, arsenene, antimonene, bismuthene) are among the most studied monoelemental materials.[3–5] Other van der Waals layered systems have been intensively investigated such as boron nitride or transition metal dichalcogenides.[6,7]

In the line of multi-elemental 2D materials, layered hydroxides (LHs) –that can clearly be regarded as 2D materials, as the in-plane growth is controllable while the thickness can be maintained to stay in the few-layer limit– provide a fascinating case of study, given the ability to tune either the chemistry of the inorganic layer and/or the (in)organic nature of the interlayer space, placing them in a prime position for energy storage and conversion, hybrid materials and magnetic devices.[8–12] Layered double hydroxides (LDHs) spotlight as one of the few examples of positively charged 2D materials, consisting of both M^{II} and M^{III} octahedral cations with purely electrostatic sheet-anion interaction.[13,14] These features have allowed to preparation of multifunctional LDHs owing a plethora of properties which result in their application in different fields such as energy storage, catalysis, anion exchange, or magnetism, among others.[15] In contrast, other members of the LHs family much less studied, such as α– and β–hydroxides, present exclusively van der Waals interactions . The former ones, depict very interesting features such as expanded structures with a rich interlayer chemistry (as in the case of LDHs), being among the most important electroactive phases based on earth-abundant metals for application in water splitting and supercapacitive devices.[16] However, unlike LDHs, α–hydroxides consist in non-charged layers. Moreover, concerning the magnetism, α-hydroxides present a versatile 2D magnetic behaviour showing considerably higher ordering temperatures, remnant magnetizations and coercive fields than the analogous LDHs. Therefore, they are appealing building blocks for the construction of multi-functional hybrid architectures.[17,18]

The structure of α-Co hydroxides (or *Simonkolleite*-like structures, a basic salt) consists of layers with Co^{II} cations located in octahedral –Co^{II}(O_h)– and tetrahedral –Co^{II}(T_d)– coordination environments (Scheme 1). While Co^{II}(O_h) are placed within the layers, Co^{II}(T_d) are attached to the inorganic sheets on both sides of the basal plane through 3 OH bridges. The fourth position, considered as a chemical functionalization, can be used to graft different ligands, ranging from inorganic to organic molecules (Scheme 1C).[19] Interestingly, the electronic and magnetic properties of α-Co hydroxides can be chemically modulated by controlling the grafted molecules and/or Co^{II}(T_d) ratio, resulting in systems with tuneable band gaps, mainly due to ligand to metal charge transfer.[20,21] Additionally, this kind of phases, and those containing Co and Ni, are very promising electroactive earth-abundant systems for energy storage and conversion.[16] However, the synthesis of α-Co hydroxides with a precise control of the morphology is far from being straightforward, as

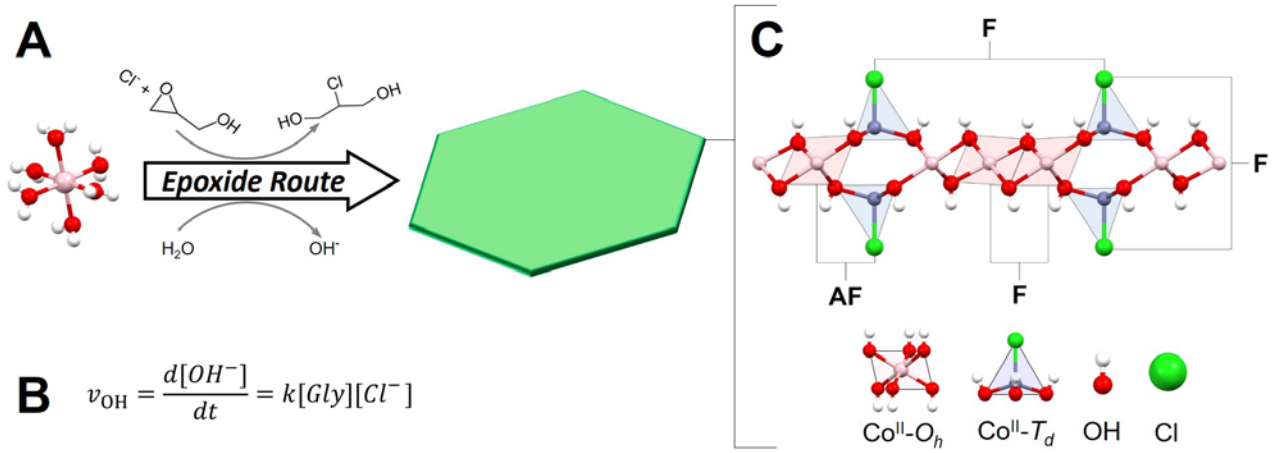

Scheme 1. Bottom up approach for the synthesis of a 2D hexagonal crystalline α-Co^{II} hydroxychloride phase. The synthetic method is based on the mild homogeneous reaction taking place at room temperature by the nucleophilic attack of chloride over glycidol: the *epoxide route* (A). The alkalinization reaction can be adjusted by changing both glycidol and chloride concentrations (B). The crystalline structure of this 2D layered hydroxide consists in layers, composed by Co^{II} in octahedral (pink) and tetrahedral (purple) coordination environments, connected by hydroxy bridges (oxygen in red, hydrogen in white). The grafted ligand is chloride (green). These 2D ferrimagnets present both, in-plane ferromagnetic (F) and antiferromagnetic (AF) interactions (C)

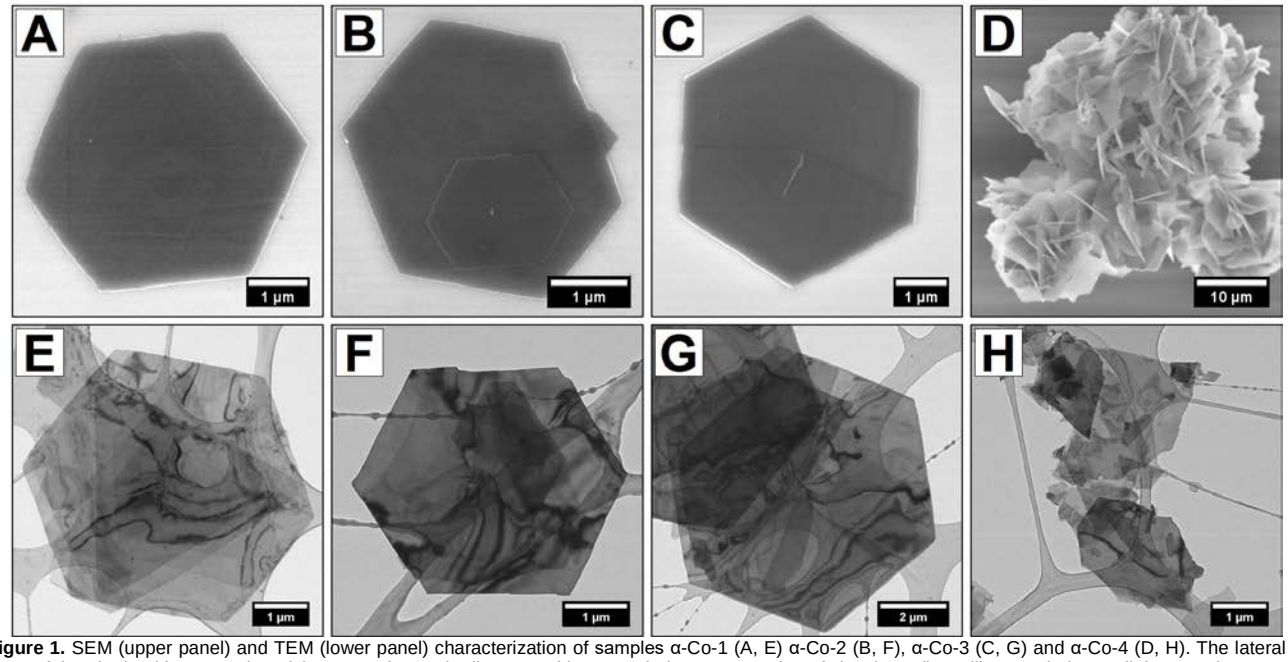

Figure 1. SEM (upper panel) and TEM (lower panel) characterization of samples α-Co-1 (A, E) α-Co-2 (B, F), α-Co-3 (C, G) and α-Co-4 (D, H). The lateral sizes of the obtained hexagonal particles exceed 5 µm in diameter with α-Co-4 being an exception of showing a flowerlike morphology. All the samples were synthesized at room temperature by employing the *epoxide route*, experimental conditions are summarized in Table S1.

polycrystalline 3D flower-like morphologies are the most reported ones.[22–26] When it comes to 2D layers, the state-of-the-art synthetic method involves ammonia releasing reagents (ARRs), which require temperatures higher than 90 ºC and an inert atmosphere.[27]

Herein, we provide a straightforward, reproducible, one-pot room temperature approach to obtain 2D, highly crystalline, hexagonally shaped α-Co^{II} hydroxychloride with enormous anisotropy (aspect ratio > 250, length > 5 µm, thickness < 20 nm). This is possible thanks to a controllable increment of the pH by a simple chemical reaction in aqueous solution between chloride anions (a nucleophile) and glycidol (an epoxide): the so-called *epoxide route*.[28]

Furthermore, we have characterized the magnetic properties exhibiting almost identical magnetic behaviour as the previously reported α-Co^{II} hydroxychlorides. Indeed, they show similar spontaneous magnetization temperatures, saturation magnetization and coercive fields. Slight differences arise in the dynamic susceptibility, which we attribute to different Co(T_d) distribution, *i.e.*: Co^{Td} clustering. To shed light on this clustering behaviour we have complemented our experimental results with a microscopic structural description based on DFT calculations.

In overall, this work provides a highly reproducible straightforward synthetic approach to obtain α-Co^{II} layered hydroxides of valuable interest for energy and magnetism, among others.

The 2D α-Co^{II} hydroxychloride hexagonal particles were obtained thanks to the *epoxide route*.[28] This mild homogeneous alkalinization method is based on a nucleophilic attack of chloride anions (a nucleophile) over the electrophilic carbon of glycidol (an epoxide), as depicted in Scheme 1. In contrast to the hydrolysis of ammonia releasing reagents (ARRs),[29] this reaction increases the pH, even at room temperature and atmospheric conditions, triggering the precipitation of several layered hydroxides and their hybrid forms.[30] The alkalinization rate, and subsequent precipitation, can be modulated easily by changing either the chloride or glycidol concentrations. Hence, the rate factor, defined as the product between both concentrations ($f_{vel} = [Cl^-][Gly]$), can be used to control the precipitation time (Scheme 1).

We have previously demonstrated the obtaining of flower-like α-Co^{II} and Ni^{II} hydroxychloride phases by employing high f_{vel} and chloride concentration.[23] Moreover, we reported the synthesis of the entire family of α-Co^{II} hydroxyhalides (with F, Cl, Br and I) in the form of single-crystalline hexagonal platelets of 1–3 µm diameter, with a variable degree of coalescence or twinning, at low halide and glycidol concentrations.[20] It is important to remark that syntheses based on ARRs do not allow the isolation of pure α-Co^{II} hydroxides, containing other anions than chlorides, pinpointing the *epoxide route* in a privileged position for the synthesis of α-Co^{II} hydroxides.[20,31]

We hypothesize that by reducing both, f_{vel} and the ionic strength (*i.e.*: chloride concentration), a better morphological control will be possible leading to highly anisotropic 2D hexagonal particles, as in the case of the report of Sasaki's team.[27] Therefore, four synthetic scenarios were evaluated (see Table S1), employing chloride and glycidol concentrations in the range of 50–500 and 100–400 mM, respectively. In all the cases, the Co^{II} concentration was fixed to be 10 mM (see Experimental Section in SI).

In contrast to hydrothermal methods, the syntheses based on the *epoxide route* are fairly simple. Only three steps are required: (*i*) preparation of stock solutions of $CoCl_2.6H_2O$ and NaCl at 250 and 2000 mM, respectively, adjusted to pH=3 with HCl. (*ii*) Mixing the stock solutions to obtain the desired initial concentrations. (*iii*) Finally, adding glycidol under continuous magnetic stirring. It is important to note that the reaction starts with the addition of the glycidol. The synthesis can be carried out either in plastic or glass flasks and without appreciable changes by increasing the volume (we have successfully carried out experiments from 1 mL to 10 L).

To assess the morphology of the materials we conducted a microscopic characterization (SEM and TEM), presented in Figure 1. Upon variation of the rate factor f_{vel} and chloride concentration, the hexagonal form of the crystals is maintained for α-Co-1 to α-Co-3 (Figure 1A-C, E-G). However, in the case of α-Co-4, at higher chloride concentration (500 mM), mainly flower-like aggregates are observed (Fig. 1D, H). In bright field (BF) TEM (Fig. 1E-H) clear bend contours are an indication of deformation of the crystals, owed to their extremely low thicknesses. For all investigated materials the lateral sizes exceed 5 µm.

Samples α-Co-1 (hexagonal crystals) and α-Co-4 (flower-like crystals), synthetized at room temperature, were characterized and compared to α-Co(HT)-H (hexagonal crystals) and α-Co(HT)-F (flower-like), obtained by employing a hydrothermal process based on ARR.[27] The characterization of all samples can be found in the SI.

Figure 2A depicts the PXRD patterns where it is possible to confirm the occurrence of *Simonkolleite*-like structure in all cases.

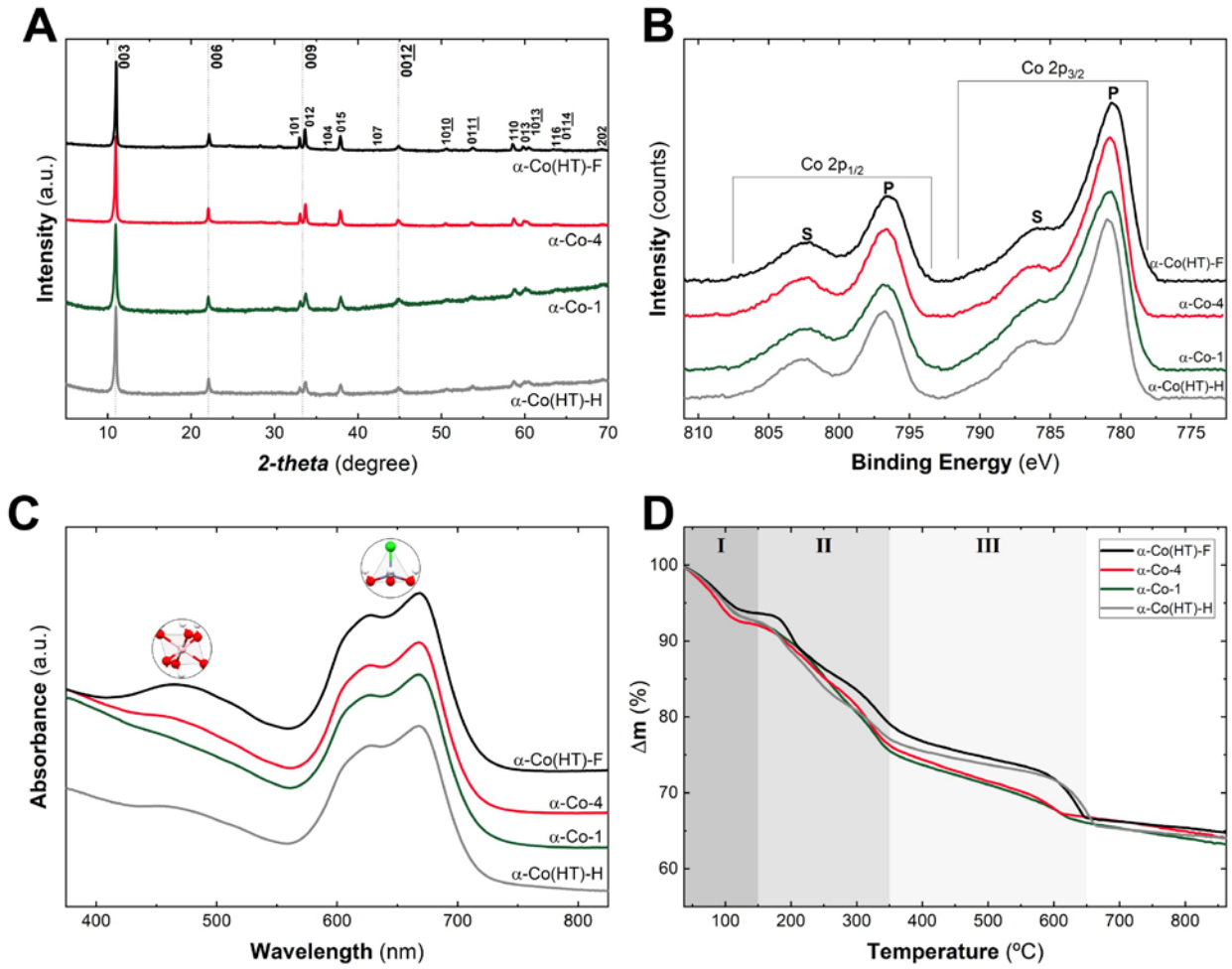

Figure 2. PXRD patterns indexed according to reference 18 (A), high resolution XPS for Co 2p ($2p^{3/2}$ and $2p^{1/2}$) in the range 810 – 775 eV (B), and UV-Vis diffuse reflectance spectra for α-Co samples. TGA thermograms under inert atmosphere (He, 20 mL/min) for α-Co samples. Mass loss step are assigned to the: dehydration (I), dehydroxylation (II), and chloride release (III) processes. In all the case the final product corresponds to *fcc* CoO.

From the (*00l*) and (*110*) reflections, basal space and intralayer (*a* parameter) distances of 8.06 Å and 3.14 Å are obtained. Figure S1 compiles the PXRD patterns of the other samples synthesized at room temperature. Remarkably, despite the samples were obtained at room temperature, the quality of the diffractograms reveal highly crystalline layered materials, as it is possible to confirm in comparison with samples from the hydrothermal process (>90 ºC). This fact is attributed to the high rate constant for water exchange in the case of Co^{II},[32] which ensures the crystallization of Co-based hydroxides even without a recrystallization process.[20,22,23,30,31,33]

We performed X-ray photoelectron spectroscopy (XPS) to gain further information about the chemical speciation and composition of the samples (Figure 2B). The presence of Co^{II} is supported by its main peaks at 780.7±0.1 eV ($2p^{3/2}$) and 796.7±0.1 eV ($2p^{1/2}$), and their satellites at 786.1±0.1 eV and 802.6±0.1 eV, respectively (for more details regarding the XPS fittings, see Figure S2-3 and Table S2).[34] No differences are observed either by changing the initial conditions or in respect to the hydrothermal samples (Figure S4). In order to provide more information related to the coordination environments for Co^{II}, octahedral and tetrahedral sites, LHs, containing only Co^{II}(O_h) were synthetized hydrothermally. Figure S5 present the XPS spectra for β-$Co(OH)_2$ and CoAl LDH in comparison to sample α-Co-1. No appreciable differences are noticeable, suggesting that XPS is not the most appropriate technique to identify Co^{II} coordination environments in LHs.

Thus, we employed UV-Vis diffuse reflectance spectroscopy to gain further insight into the different coordination environments for Co^{II} (Figure 2C). In all cases, a broad and almost indistinguishable band around 470–530 nm can be assigned to Co^{II}(O_h). Moreover, the appearance of a strong band with twin-peaks centred at 628 nm and 668 nm confirms the presence of Co^{II}(T_d) in all the cases (Figure S6).[19,20,22,35] Hence, due to the high sensitivity of this Co^{II}(T_d) absorption band with respect to the coordinated anion, this technique qualifies as the most suitable tool to identify either cationic coordination environments[30,35] and/or the nature of the functionalized and/or coordinated anion[20,31] in Co-based LHs.

To gain further information regarding the thermal stability of the α-Co^{II} hydroxychlorides, we carried out TGA measurements. We followed the thermal decomposition under inert atmosphere (He, 20 mL/min) from room temperature up to 900 ºC at 10 ºC/min. After the TG measurements, for all samples, PXRD patterns of the remnant solids confirm the generation of crystalline *fcc* Co^{II} oxide (CoO). XPS confirms the absence of chloride (data not shown), in agreement with previous reports on hydroxyhalide phases under oxidizing conditions.[20,27] The thermograms are practically identical in all cases, denoting three well-defined mass loss steps (Figure 2D). The first mass loss, ascribable to the physisorbed water, takes place at 90±2 ºC, in concordance with previous reports for purely inorganic[20] or hybrid[31,36] α-Co^{II} hydroxide phases. The second step takes place in a wide temperature range from *ca.* 150 to 375 ºC, being related to the dehydroxylation of the structural OH groups belonging to the layered phases, triggering the collapse of the layered structure.[20,36,37] The analysis of the first derivative confirms the presence of three less-defined processes taking place in this second step at 191±7, 240±8 and 326±5 ºC, respectively (see

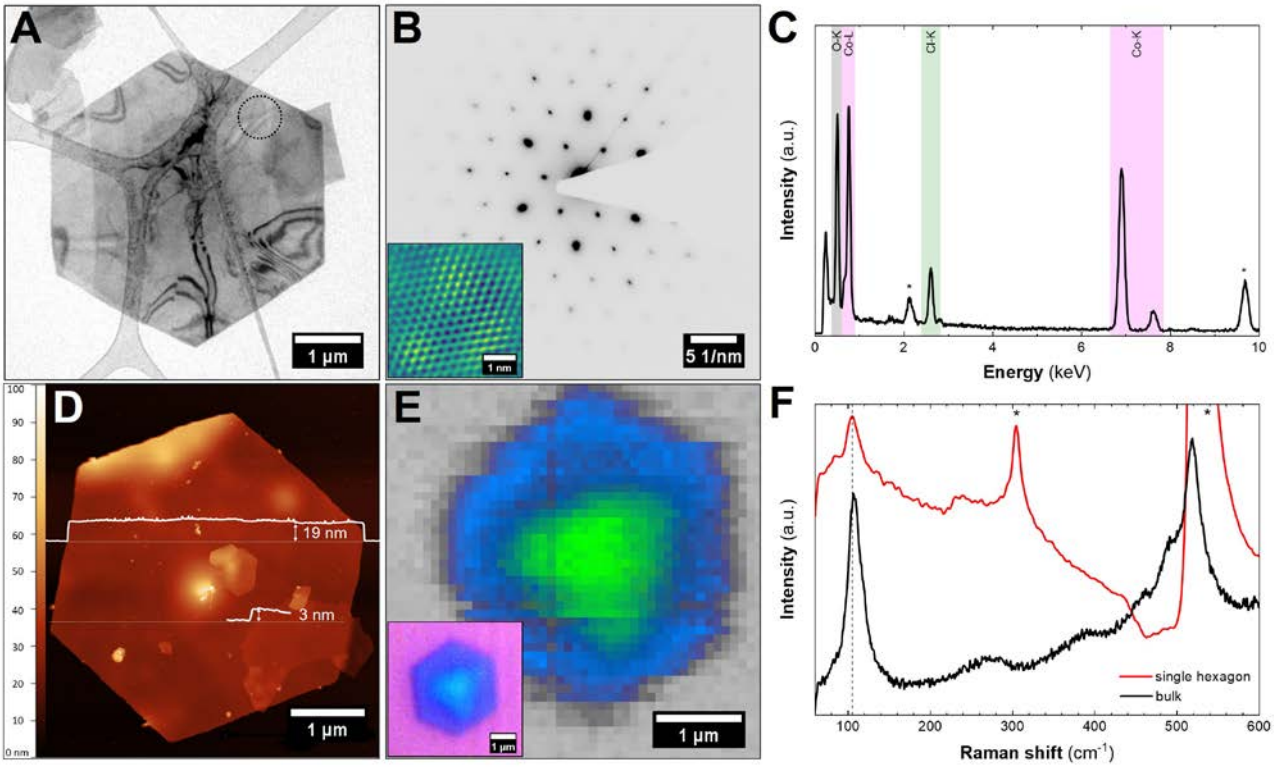

Figure 3. BF-TEM of individual α-Co-1 hexagonal particle, circle indicates position for the placement of the SA aperture (A). SAED pattern showing hexagonal in-plane order. Inset shows a FFT-filtered HRTEM image reproducing the hexagonal order of the crystalline lattice (B). EDS spectrum acquired in TEM, indicating O, Co and Cl as the main constituents (peaks marked with an asteriks are stray signals from the TEM Au grid) (C). AFM image revealing a homogenous thickness of ca. 19 nm over the whole hexagonal particle with an additional layer of 3 nm thickness (D). Scanning Raman mapping of individual hexagonal particle with optical microscopy image as insert. In the central region an additional triangular layer on the hexagonal flake can be noticed (E). Raman point spectra comparing an individual α-Co-1 hexagonal particle on Si (red, asteriks indicates signals from SiO_x wafer) to the bulk material (black). Peaks located at Raman shifts >200 cm^{-1} overlap with the SiO_x substrate while the signal at 105 cm^{-1} is a clear indication for the probing of α-Co-1 (F).

Figure S7-8 and Table S3). Finally, at 620±19 ºC, the last mass loss step can be assigned to the chloride atoms departure.[20] Only in this case we noted a slight shift to higher temperature of less than 40 ºC, for samples obtained hydrothermally which is probably related to the layer thicknesses of those samples (Figure 3D, S8 and Table S3). Additionally, for TGA measurements carried out under oxidizing atmosphere (synthetic air, 100 mL/min), analogous profiles are observed, while the whole decomposition process, resulting in the generation of Co_3O_4, occurs at temperatures lower than 350 ºC (Figure S9).[27]

All techniques confirm pure *Simonkolleite*-like α-Co^{II} hydroxychloride phases without differences between our samples and those synthesized hydrothermally. To assess the Cl:Co ratio, ICP is not a suitable technique, therefore we used the averages of EDS and XPS techniques[22] to estimate the amount of $Co^{II}(T_d)$ being 27±3 %, for all cases (see Table S4). To summarize, the establishment of α-Co^{II} layered hydroxides in the form of $Co^{Oh}_{0.73}Co^{Td}_{0.27}(OH)_{1.73}Cl_{0.27} \cdot 0.5H_2O$ can be safely concluded.

Once identified that our samples are pure α-Co^{II} hydroxychloride we chose α-Co-1 as a representative member of the α-Co family and subjected it to further investigation with microscopic techniques, summarized in Figure 3. Figure 3A shows a BF-TEM image of one hexagonal particle highlighting with a circle selected area for the electron diffraction (SAED) analysis shown in Figure 3B. The SAED pattern, taken along [*00l*] direction, clearly reveals the single crystalline structure of the nanosheet, resembling a hexagonal ordering within the basal plane. The inset in Figure 3B shows a filtered and colorized HRTEM image of the hexagonal lattice at atomic resolution, confirming the structure on the atomic scale. In Figure 3C the EDS spectrum, acquired over one hexagonal particle in TEM confirms the composition of the material, showing O, Co and Cl (mind the Au-M and Au-L signals marked with asterisk, stemming from the employed Au-TEM grid). The AFM data in Figure 3D indicates a thickness of 19 nm, while the length exceeds 5 µm. A step of 3 nm thickness indicates the presence of an additional few-layer α-Co-1 nanosheet. The analysis over >30 nanosheets reveal an average thickness of 20±7 nm. Interestingly, by comparing edge-to-egde (6.4±1.7µm) and side-to-side (5.7±1.5µm) measurements we can confirm highly symmetric hexagonal particles with an edge-to-side ratio of *ca.* 0.89 (see Figure S10-11 and Table S5). This results in an impressive size-thickness relationship ($2.6 \cdot 10^7$ nm^2 per 25 atomic layers), clearly outperforming in three orders of magnitude any previous liquid phase exfoliated layered hydroxide reported to date.[38,39] In Figure 3E, a spatially resolved Raman mapping and the corresponding optical microscopy image as inset are shown. The colour scale is based on a least square fitting of reference spectra extracted from the respective regions (Si wafer, outer rim and inner triangular adlayer). The extracted spectrum from the α-Co-1 hexagonal particle on a Si wafer is compared to the bulk material in Figure 3F, where the asterisks in the red spectrum of the individual hexagonal particle indicate Raman signals ascribable to the SiO_x substrate (see SI for further information). Unfortunately, almost the whole fingerprint region of α-Co-1 is overlapped by the SiO_x induced signals. Nevertheless, the peak at 105 cm^{-1} gives a clear handle on identifying the material. We compared these results with the Raman spectra from CoO and Co_3O_4 to avoid the assignment of the spectra to the oxidized species (Figure S12) and can clearly state that observed material can be regarded as α-Co-1 without measurable oxidation.

Regarding the magnetism, this layered structure is quite interesting. Generally, there are two main contributions associated with the magnetism in layered hydroxides: first, purely in-plane intralayer magnetic coupling between the cations, mediated by superexchange interactions through hydroxy bridges. Secondly, a less intense out-of-plane interlayer dipolar interaction, strongly dependent on the d_{BS}. Nevertheless, α-Co^{II} hydroxides are characterized by presenting a more complex

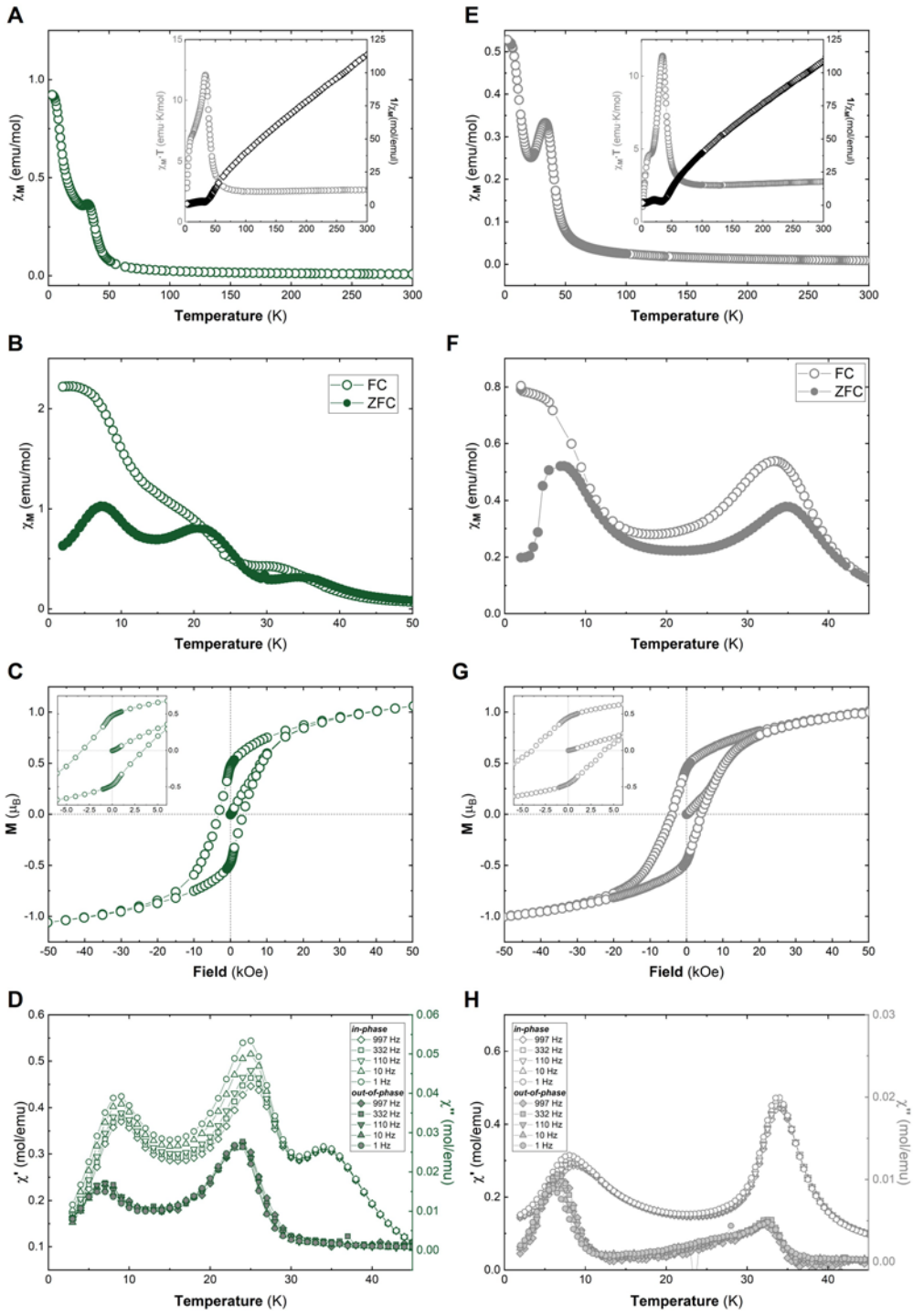

Figure 4. Magnetic characterization for α-Co-01 (left panel, green) and α-Co(HT)-H (right panel, grey) samples containing chloride as interlayer anion. Magnetic susceptibility as a function of temperature (χ_M *vs* T) with an external applied field of 1000 Oe; the inset represents the thermal dependence of χ_M·T and the fitting of the 1/χ_M to a Curie–Weiss law (A and E). FC/ZFC with an external applied field of 100 Oe (B and F). Hysteresis cycle at 2 K; the inset depicts the low field region (C and G). Thermal dependence of dynamic susceptibility for the in-phase (χ_M') and' the out-of-phase (χ_M'') signals at 1, 10, 110, 332 and 997 Hz (D and H).

behaviour, mainly by the occurrence of different magnetic sublattices arising from the diverse Co environments.[20,40] Precisely, ferromagnetic (F) interactions between Co in identical coordination environments (O_h–O_h and T_d–T_d) and antiferromagnetic (AF) interactions between Co in different environments (O_h–T_d) are expected (see Scheme 1C). The uncompensated moments inherent to this scenario, also known as triple deck structures,[17] result in ferrimagnetic layers.[40] As it was reported for α-Co^{II} hydroxychlorides and α-Co^{II} hydroxyhalides, the overall magnetism depend mainly on the amount of $Co^{II}(T_d)$.[20] Nevertheless, as we have recently reported, in the case of hybrid α-Co^{II} hydroxydicarboxylates, $Co_5(OH)_8[(CH_2)_n(COO)_2]$ with *n* from 1 to 8, the magnetic behaviour can be dramatically modified by changing the parity of the organic linker: while odd members present T_M < 20 K the even ones have T_M > 55 K, exclusively, even with a fixed amount of $Co^{II}(T_d)$. This is related to the torsions in the orientation of the carboxylic groups and the Co^{Td}-O_{COO} distances.[31]

The magnetic experimental results for each sample are summarized in Figures S13-18 and Table S6, while Figure 4 and

Table 1. Main magnetic data and parameters for α-Co^{II} hydroxychloride phases. $\chi \cdot T_{RT}$ value at room temperature; experimental Curie constant (C); Weiss constant (θ); temperature of the divergence of the ZFC and FC magnetic susceptibility (T_B); temperature for the onset of spontaneous magnetization extracted from the χ''_M plot (T_M); saturation magnetization (M_S); remanence magnetization (M_R); coercive field (H_C).

Samples	$\chi \cdot T_{RT}$ (emu·K/mol)	C (emu·K/mol)	θ (K)	T_B (K)	T_M (K)	M_S (μ_B)	M_R (μ_B)	H_C (Oe)
α-Co-01	2.64	2.8	21.2	31.5	33.8	1.06	0.47	3428
α-Co(HT)-H	2.75	3.1	38.7	32.7	36.5	1.00	0.45	3938

Table 1 compile the main relevant parameters for the hexagonal particles, α-Co-1 *vs* α-Co(HT)-H. It is important to point out that the magnetism of this hydrothermally synthesized crystal has never been reported before. Generally, all samples present a similar magnetic behaviour (Table S6), as expected according to the structural characterization. The DC susceptibility measurements (χ_M) exhibit a continuous increase upon cooling, with a pronounced growth starting at *ca.* 45 K. Moreover, the $\chi_M \cdot T$ product also increases, exhibiting a sharp peak at around 34 K (Figure 4A and 4E). From the temperature-independent component in $\chi_M \cdot T$, the absence of extrinsic magnetic impurities such as Co^{III} spinels can be confirmed, highlighting the phase purity in all the cases (Figure 4, inset).[41,42]

To gain deeper insights into the magnetic behaviour, the inverse of the magnetic susceptibility ($1/\chi$) can be fitted according to a Curie–Weiss law in the 200–300 K region (Figure 4, inset). In all cases an overall ferromagnetic behaviour can be deduced by $\theta_{CW} > 0$, in agreement with previous reports for α-Co^{II} hydroxychlorides with $Co^{II}(T_d)$ lower than 0.3 (Table 1).[20,40] Furthermore, by plotting the data for C and θ_{CW} according to equation (1):

$$\frac{C}{\chi|\theta_{CW}|} + sgn(\theta_{CW}) = \frac{T}{\theta_{CW}} \qquad \text{(eq.1)}$$

positive and negative deflections from the ideal θ_{CW} behaviour can be clearly observed, which are indicative of compensated and uncompensated interactions, respectively.[40] In all cases, the observed compensated interactions suggest AF coupling between the layers (Figure S19).[20,40] From field-cooled and zero field-cooled (FC/FZC) DC measurements we extracted blocking temperatures (T_B) centred around 32 K (Figure 4B and 4F). In dynamic AC susceptibility measurements (in-phase and out-of-phase), magnetization temperatures below 40 K are determined (Figure 4D and 4H, T_M, defined as the point in which $\chi''_M \neq 0$). Hysteresis loops recorded at 2 K further confirm the spontaneous magnetization, where a large spin-orbit coupling is evidenced by the magnitude of the coercive field (H_c). In all cases we observed H_c higher than 3400 Oe (Figure 4C and G).[43]

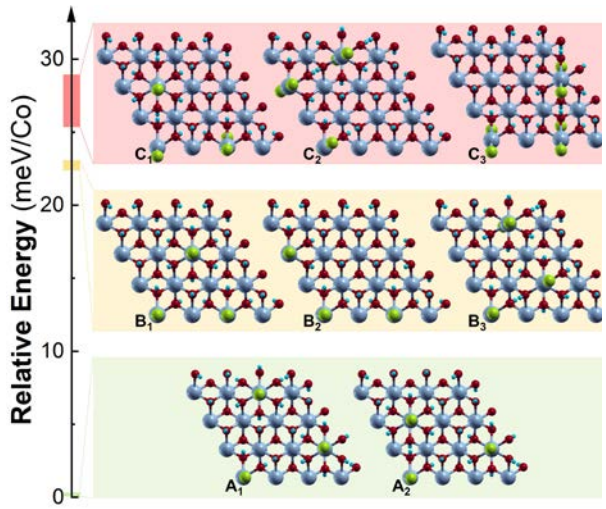

Figure 5. Relative energy expressed as meV/Co as a function of the different evaluated Co^{Td}-clusters. According to the relative energy of each of one, three groups are defined.

So far, all the samples seem to be identical in terms of the overall magnetic behaviour without clear correlations either by the initial synthetic conditions nor the recrystallization process, in perfect agreement with previous reports.[20,40]

However, by analysing in detail the FC/ZFC and in-phase/out-of-phase dynamic AC susceptibility, different magnetic features can be observed, highlighting the complex magnetic structure of this type of compounds.[40] Indeed, while sample α-Co-1 presents three peaks at 9, 25 and 34 K, in the case of sample α-Co(HT)-H the broad peak at 25 K is missing. Additionally, different dependences with the frequency are observed. These results suggest the presence of different sublattices or microdomains,[40] which could be modified due to the synthetic conditions, even for an identical chemical composition.

Taking advantage of our previous experience in the description of these layered hydroxides by DFT+U simulations,[20,21,31,35,44] we decided to tackle this complex structural scenario studying the possibility of having different $Co^{II}(T_d)$ spatial distributions within the layers, *i.e.*: in-plane Co^{Td}-clustering. In this line, a supercell with the general formula $Co_{13}^{Oh}Co_6^{Td}(OH)_{32}Cl_6$ was employed to generate different Co^{Td}-clusters. In all cases, F coupling between Co atoms in the same environment, and AF coupling between the $Co^{II}(T_d)$ and $Co^{II}(O_h)$ atoms were contemplated. Considering symmetry restrictions, we identified eight representative superstructures (*i.e.*: Co^{Td}-clusters). Due to the high energy for neighbouring Co^{Td} sites as a consequence of the Cl–Cl steric repulsion (~150 meV), those clusters were excluded.[31] After performing the atomic relaxation of the structures, the relative energy for each Co^{Td}-cluster, expressed per Co atom (meV/Co), provides a tool to divide them in three groups (A, B and C). Figure 5 compiles the simulated structures; the energy values can be found in Table S7. While group A presents the lowest relative energies (<0.5 meV), groups B and C depict energy values higher than 20 meV. These results seem to suggest that the stability of the Co^{Td}-clusters is strongly correlated with the distance between the $Co^{II}(T_d)$ moieties, mainly affected by Cl–Cl steric repulsion. However, taking into account that the energy differences between these three cluster groups (A, B and C) are around the thermal energy at room temperature (kT ~ 25 meV), all of them represent accessible conformations/states for the system from a thermodynamic point of view. Hence, the synthetic conditions (alkalinization rate, chloride concentration, temperature) can modify the Co^{Td} clustering. These results are in line with the report of Nielson *et al.* who showed the presence of distinct clustering in α-Co^{II} hydroxychlorides synthesized at room temperature when different Co^{Td}:Co^{Oh} ratios are compared, by employing synchrotron X-ray total scattering.[45]

Clustering in LHs is an interesting topic that deserves to be explored. For instance, in the case of NiFe LDHs, Fe^{III}-clustering results in a spin frustration[46] which affects the catalytic behaviour of Fe centres for the water splitting reaction.[47] In fact, in the case of ZnAl LDHs, Nielsen *et al*. have reported how the effect of the synthesis (pH, metal ion concentration, and post-synthesis treatment) can affect the local (atomic) and global structure.[48] By employing solid state ^{1}H, ^{27}Al and ^{67}Zn NMR, they have demonstrated that a careful pH control, followed by hydrothermal treatment is the most appropriated pathway to avoid Al-rich phases (Al^{III}-clustering). Hence, the magnetic transition at *ca.* 35 K observed for α-Co^{II} hydroxychlorides hydrothermally synthesized could suggest that under high temperature conditions the system is able to recrystallize toward the most stable scenario,

minimizing the clustering (*i.e.*: Cl–Cl steric repulsion). In any case, these results would need to be contrasted with other techniques, especially studying individual single crystals, trying to understand the role of the Co^{Td}-clustering on the electronic structure, which might affect magnetism or electrocatalytic performance.

In conclusion, we presented the room temperature bottom-up synthesis of ultrathin layered hexagonal magnets based on α-Co^{II} hydroxychlorides exhibiting diameters higher than 5 μm and thicknesses of 20±7nm, with a very high aspect ratio of >250. This synthetic approach, based on the *epoxide route* is extremely easy, highly reproducible, and scalable. In addition, by tuning the initial synthetic conditions, other particle shapes and sizes can be obtained. These 2D multilayers behave as ferrimagnets with magnetization temperatures of *ca*. 33K and coercive fields >3400 Oe. Interestingly, even if the initial conditions do not affect the chemical composition, magnetic characterization and DFT+U calculations alert about different magnetic sublattices or microdomains as a consequence of distinct Co^{Td} clustering.
This work outperforms any liquid phase exfoliated layered hydroxide reported to date in terms of size-thickness relationship by at least three orders of magnitude,[38,39] thus paving the way for the development of 2D α-Co^{II} nanomaterials applications.

Acknowledgements

This work was supported by the European Research Council (ERC Starting Grant No. 2D-PnictoChem 804110), the Spanish MICINN (PID2019-111742GA-I00 and Unit of Excellence "María de Maeztu" CEX2019-000919-M), the Deutsche Forschungsgemeinschaft DFG (FLAG-ERA AB694/2-1), the Generalitat Valenciana (CIDEGENT/2018/001) and iDiFEDER/2018/061 co-financed by FEDER. D.H. acknowledges CONICET for financial support and CNEA Computing Clusters for computer time (density functional theory calculations). Authors thanks to Dr. G. Agustí and Dr. J. M. Martínez for magnetic measurements, and Dr M. D. Jordán Martín for her kind assistance with the XPS measurements. V.O. is member of ALN.

Keywords: two-dimensional (2D) materials • layered hydroxides • hexagonal morphology • bottom-up synthesis • magnetism

[1] F. Bonaccorso, L. Colombo, G. Yu, M. Stoller, V. Tozzini, A. C. Ferrari, R. S. Ruoff, V. Pellegrini, *Science* **2015**, *347*, DOI 10.1126/science.1246501.
[2] M. Gibertini, M. Koperski, A. F. Morpurgo, K. S. Novoselov, *Nature Nanotechnology* **2019**, *14*, 408–419.
[3] P. Ares, J. J. Palacios, G. Abellán, J. Gómez-Herrero, F. Zamora, *Advanced Materials* **2018**, *30*, 1703771.
[4] J. Sturala, Z. Sofer, M. Pumera, *Angewandte Chemie International Edition* **2019**, *58*, 7551–7557.
[5] P. Vishnoi, K. Pramoda, C. N. R. Rao, *ChemNanoMat* **2019**, *5*, 1062–1091.
[6] C. Tan, X. Cao, X.-J. Wu, Q. He, J. Yang, X. Zhang, J. Chen, W. Zhao, S. Han, G.-H. Nam, M. Sindoro, H. Zhang, *Chem. Rev.* **2017**, *117*, 6225–6331.
[7] X. Kong, Q. Liu, C. Zhang, Z. Peng, Q. Chen, *Chem. Soc. Rev.* **2017**, *46*, 2127–2157.
[8] J. Azadmanjiri, J. Wang, C. C. Berndt, A. Yu, *J. Mater. Chem. A* **2018**, *6*, 3824–3849.
[9] R. Patel, J. Tae Park, M. Patel, J. Kumar Dash, E. Bhoje Gowd, R. Karpoormath, A. Mishra, J. Kwak, J. Hak Kim, *Journal of Materials Chemistry A* **2018**, *6*, 12–29.
[10] Y. Liu, N. O. Weiss, X. Duan, H.-C. Cheng, Y. Huang, X. Duan, *Nature Reviews Materials* **2016**, *1*, 1–17.
[11] W. Zhang, Q. Wang, Y. Chen, Z. Wang, A. T. S. Wee, *2D Mater.* **2016**, *3*, 022001.
[12] G. Abellán, C. Martí-Gastaldo, A. Ribera, E. Coronado, *Acc. Chem. Res.* **2015**, *48*, 1601–1611.
[13] J. Yu, Q. Wang, D. O'Hare, L. Sun, *Chem. Soc. Rev.* **2017**, *46*, 5950–5974.
[14] G. Abellán, E. Coronado, C. Martí-Gastaldo, E. Pinilla-Cienfuegos, A. Ribera, *J. Mater. Chem.* **2010**, *20*, 7451–7455.
[15] G. Fan, F. Li, D. G. Evans, X. Duan, *Chem. Soc. Rev.* **2014**, *43*, 7040–7066.
[16] I. Roger, M. A. Shipman, M. D. Symes, *Nature Reviews Chemistry* **2017**, *1*, 1–13.
[17] G. Rogez, C. Massobrio, P. Rabu, M. Drillon, *Chem. Soc. Rev.* **2011**, *40*, 1031–1058.
[18] P. Rabu, E. Delahaye, G. Rogez, *Nanotechnology Reviews* **2015**, *4*, 557–580.
[19] R. Ma, Z. Liu, K. Takada, K. Fukuda, Y. Ebina, Y. Bando, T. Sasaki, *Inorg. Chem.* **2006**, *45*, 3964–3969.
[20] V. Oestreicher, D. Hunt, R. Torres-Cavanillas, G. Abellán, D. A. Scherlis, M. Jobbágy, *Inorg. Chem.* **2019**, *58*, 9414–9424.
[21] D. Hunt, M. Jobbagy, D. A. Scherlis, *Inorg. Chem.* **2018**, *57*, 4989–4996.
[22] J. R. Neilson, B. Schwenzer, R. Seshadri, D. E. Morse, *Inorg. Chem.* **2009**, *48*, 11017–11023.
[23] N. Arencibia, V. Oestreicher, F. A. Viva, M. Jobbágy, *RSC Advances* **2017**, *7*, 5595–5600.
[24] H. Zhang, W. Tian, X. Guo, L. Zhou, H. Sun, M. O. Tadé, S. Wang, *ACS Appl. Mater. Interfaces* **2016**, *8*, 35203–35212.
[25] T. Dong, X. Zhang, M. Li, P. Wang, P. Yang, *Inorg. Chem. Front.* **2018**, *5*, 3033–3041.
[26] E. Boccalon, G. Gorrasi, M. Nocchetti, *Advances in Colloid and Interface Science* **2020**, *285*, 102284.
[27] Z. Liu, R. Ma, M. Osada, K. Takada, T. Sasaki, *J. Am. Chem. Soc.* **2005**, *127*, 13869–13874.
[28] V. Oestreicher, M. Jobbágy, *Langmuir* **2013**, *29*, 12104–12109.
[29] K. Okamoto, N. Iyi, T. Sasaki, *Applied Clay Science* **2007**, *37*, 23–31.
[30] V. Oestreicher, M. Jobbágy, *Chemistry – A European Journal* **2019**, *25*, 12611–12619.
[31] Oestreicher, Víctor, Hunt, Diego, Dolle, Christian, Borovik, Paula, M. Jobbágy, G. Abellán, E. Coronado, *Chemistry – A European Journal* **2020**, DOI accepted.
[32] F. A. Dunand, L. Helm, A. E. Merbach, in *Advances in Inorganic Chemistry*, Academic Press, **2003**, pp. 1–69.
[33] V. Oestreicher, I. Fábregas, M. Jobbágy, *J. Phys. Chem. C* **2014**, *118*, 30274–30281.
[34] M. C. Biesinger, B. P. Payne, A. P. Grosvenor, L. W. M. Lau, A. R. Gerson, R. St. C. Smart, *Applied Surface Science* **2011**, *257*, 2717–2730.
[35] V. Oestreicher, D. Hunt, M. Mizrahi, F. G. Requejo, M. Jobbágy, *Chemistry – A European Journal* **2020**, *n/a*, DOI 10.1002/chem.202001944.
[36] V. Oestreicher, G. Abellán, E. Coronado, *physica status solidi (RRL) – Rapid Research Letters* **n.d.**, *n/a*, DOI 10.1002/pssr.202000380.
[37] J. A. Carrasco, A. Seijas-Da Silva, V. Oestreicher, J. Romero, B. G. Márkus, F. Simon, B. J. C. Vieira, J. C. Waerenborgh, G. Abellán, E. Coronado, *Chemistry – A European Journal* **2020**, *26*, 6504–6517.
[38] J. A. Carrasco, A. Harvey, D. Hanlon, V. Lloret, D. McAteer, R. Sanchis-Gual, A. Hirsch, F. Hauke, G. Abellán, J. N. Coleman, E. Coronado, *Chem. Commun.* **2019**, *55*, 3315–3318.
[39] C. Backes, D. Campi, B. M. Szydlowska, K. Synnatschke, E. Ojala, F. Rashvand, A. Harvey, A. Griffin, Z. Sofer, N. Marzari, J. N. Coleman, D. D. O'Regan, *ACS Nano* **2019**, *13*, 7050–7061.
[40] J. R. Neilson, D. E. Morse, B. C. Melot, D. P. Shoemaker, J. A. Kurzman, R. Seshadri, *Phys. Rev. B* **2011**, *83*, 094418.
[41] A. S.-D. Silva, R. Sanchis-Gual, J. A. Carrasco, V. Oestreicher, G. Abellán, E. Coronado, *Batteries & Supercaps* **n.d.**, *n/a*, DOI 10.1002/batt.201900223.
[42] G. Abellán, J. A. Carrasco, E. Coronado, *Inorg. Chem.* **2013**, *52*, 7828–7830.
[43] M. Kurmoo, *Chem. Mater.* **1999**, *11*, 3370–3378.
[44] D. Hunt, G. Garbarino, J. A. Rodríguez-Velamazán, V. Ferrari, M. Jobbagy, D. A. Scherlis, *Phys. Chem. Chem. Phys.* **2016**, *18*, 30407–30414.
[45] J. R. Neilson, J. A. Kurzman, R. Seshadri, D. E. Morse, *Chemistry – A European Journal* **2010**, *16*, 9998–10006.
[46] G. Abellán, E. Coronado, C. Martí-Gastaldo, J. Waerenborgh, A. Ribera, *Inorg. Chem.* **2013**, *52*, 10147–10157.
[47] D. Friebel, M. W. Louie, M. Bajdich, K. E. Sanwald, Y. Cai, A. M. Wise, M.-J. Cheng, D. Sokaras, T.-C. Weng, R. Alonso-Mori, R. C. Davis, J. R. Bargar, J. K. Nørskov, A. Nilsson, A. T. Bell, *J. Am. Chem. Soc.* **2015**, *137*, 1305–1313.
[48] S. S. C. Pushparaj, C. Forano, V. Prevot, A. S. Lipton, G. J. Rees, J. V. Hanna, U. G. Nielsen, *J. Phys. Chem. C* **2015**, *119*, 27695–27707.